COMMUNICATION

Conjugated Polymer Nanoparticles for Two-Photon Imaging of Endothelial Cells in a Tissue Model

By *Nur Aida Abdul Rahim, William McDaniel, Kevin Bardon, Shalini Srinivasan, Vernella Vickerman, Peter T. C. So,* and *Joong Ho Moon**

Two-photon (2P) imaging holds great promise for in vivo microscopic physiological studies in areas such as neurobiology, immunology, and tissue engineering.[1–3] Advances in 2P endomicroscope design have further demonstrated the possibility of developing noninvasive diagnostic procedures for the detection of malignancy in organs such as the oral cavity and the intestine.[1,4,5] Many of these applications are currently limited by a lack of fluorescent probes with large 2P action cross-sections. The availability of improved 2P fluorescent probes will enable tissue imaging with higher sensitivity, greater penetration depth, reduced tissue photodamage and tissue autofluorescence backgrounds, and lower instrument cost. Despite a number of previous efforts to design and synthesize new organic fluorophores with high 2P action cross-sections,[6–10] the utility of these probes in biomedicine has been limited by their hydrophobicity and cytotoxicity. A recent development is the realization that quantum dots (QDs) have large 2P action cross-sections on the order of 10 000 Goeppert–Mayer units (GM).[11] These QDs exhibit high photostability and narrow emission spectral width. Despite their excellent photophysical properties, broad biomedical applications of QDs are limited by drawbacks such as the existence of "dark" dots,[12] heavy-metal core-related cytotoxicity, and difficulties in surface modification.[13] Therefore, the synthesis and fabrication of alternative probes with high 2P action cross-sections is a priority.

Conjugated polymers (CPs) are attractive candidate materials that address the requirements for 2P microscopy imaging. CPs are organic materials that are readily synthesized by well-established methods.[14] Characteristic photophysical features of CPs are high fluorescence quantum yields (QYs), large extinction coefficients, and efficient energy-transfer properties.[15,16] Despite these characteristics, their intrinsic hydrophobicity originating from the π-conjugated backbone limits their potential application in biological systems. To overcome this hydrophobicity issue in cellular-imaging applications, we previously demonstrated the facile fabrication of conjugated polymer nanoparticles (CPNs) using ultrafiltration techniques.[17] Ultrafiltration of acetic acid-treated poly(*p*-phenylene ethynylene) (PPE, Scheme 1) followed by dialysis against pure water results in stable and bright CPNs 80–100 nm in size. Live cells readily uptake CPNs, which accumulate in the cytosol with no noticeable inhibition of cellular viability, even after 7 days of incubation.

In this Communication, we report on CPNs' superior 2P characteristics and 2P imaging of endothelial cells in a model-tissue culture system. Improved fabrication methods allowed dramatic reduction of CPN size, down to 8 nm. CPNs exhibit extremely large 2P cross-sections and photostability comparable to QDs. Furthermore, the hydrophilicity and nontoxicity of CPNs allow for long-term monitoring of angiogenesis by endothelial cells in a tissue model, supporting CPNs' potential in biological and biomedical applications.

CPNs were fabricated by ultrafiltration of an amine-containing PPE solution that was acidified with tartaric acid (1 M).[17] After dialysis of the solution against water, transparent yellow colored ($\lambda_{max,\ absorption} = 429$ nm, $\lambda_{max,\ emission} = 485$ nm, and QY: 0.09) CPNs were obtained (see Supporting Information for spectroscopic data, Fig. S1). The *Z*-average size of CPNs obtained from this tartaric acid treatment was significantly smaller (8 nm) than that obtained using the acetic acid treatment of the same batch of PPE solution (85 nm, see Supporting Information, Fig. S2), indicating that CPN size can be modulated by the choice of

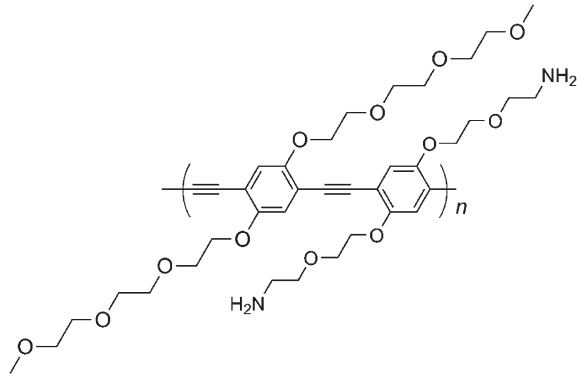

Scheme 1. Chemical structure of amine-containing PPE.

[*] Prof. J. H. Moon, S. Srinivasan
Department of Chemistry and Biochemistry
Florida International University
11200 SW 8th Street, Miami, FL 33199 (USA)
E-mail: joongho.moon@fiu.edu
N. A. A. Rahim
Department of Mechanical Engineering
Massachusetts Institute of Technology
77 Massachusetts Ave., Cambridge, MA 02139 (USA)
W. McDaniel, K. Bardon
ICx Technologies, Inc.
215 First Street, Suite 104, Cambridge, MA 02142 (USA)
V. Vickerman
Department of Chemical Engineering
Massachusetts Institute of Technology
77 Massachusetts Ave., Cambridge, MA 02139 (USA)
Prof. P. T. C. So
Department of Mechanical and Biomedical Engineering
Massachusetts Institute of Technology
77 Massachusetts Ave., Cambridge, MA 02139 (USA)

DOI: 10.1002/adma.200900416

organic acid. Bazan and coworkers[18] observed similar size changes in various solvents upon exchange of counter ions from cationic CPs. This suggests that stronger interaction between counter ions and the conjugated backbone results in smaller particles by lowering additional interaction between polymer chains. Tartaric acid (dicarboxylic acid) results in stronger interactions with the PPE's side-chain amines than acetic acid, resulting in smaller particles by reducing interaction opportunities between PPE chains. Positively charged amines, with the aid of the hydroxyl groups from tartaric acid, can provide a hydrophilic environment that prevents further aggregation driven by hydrophobic interactions between PPE chains. The CPNs fabricated from the organic acid treatment exhibit excellent stability during the first three months of storage (see Supporting Information, Fig. S3). Upon more than six months storage, we observed that the size of CPNs fabricated with the tartaric acid treatment increases to ~50 nm, while a relatively small size change (from 85 to 75 nm) was observed from the CPNs fabricated from the acetic acid treatment. We attribute the size increase in the CPNs to the aggregation of polymer chains induced by the slow leaching-out of the residual acids from the aggregates over the 6 months.[19] The small decrease in the size of CPNs from the acetic acid treatment can be explained by the limited leaching-out of the acetic acids from the relatively big CPNs, resulting in a small decrease in the size (further collapsing) due to the incremental hydrophobicity change in the CPNs. Nonetheless, the photophysical properties and cellular uptake behavior of the CPNs was not affected by the size and size distribution of CPNs fabricated using different acids.

A quadratic dependence of the fluorescence signals was observed as a function of excitation power. The log plot of counts per second (cps) versus power exhibits a linear increase with a slope of 2.0 and saturation at higher power (about 3 mW, Fig. 1a). Fluorescence correlation spectroscopy (FCS)[20] was used to quantify the number of fluorescent molecules in the excitation volume and deduce the molecular brightness of CPNs (Fig. 1b). From curve fits, the radius and diffusion time of CPNs were calculated as 3.8 nm and 382 μs, respectively. This diameter (7.6 nm) coincides well with the dynamic light scattering (DLS) *Z*-average diameter (8 nm). The 2P action cross-section of CPNs was obtained by comparing the molecular brightness of CPNs with that of fluorescein molecules with a known 2P cross-section.[21] The measured 2P-action cross-section of the CPNs as a function of excitation wavelength is shown in Figure 1c. Our measurements shows cross-sections that range between 1000 and 11 000 GM with a maximum at about 730 nm. These cross-sections are at least 2–3 orders of magnitude higher than conventional organic fluorophores. In addition, at wavelengths below 815 nm, CPNs have higher cross-section values than some QDs.[22] It is worth clarifying that the cross-section value of CPN is per particle, and is not normalized in terms of number of repeating units in the PPE used to fabricate the CPNs. This high cross-section ensures that CPNs can be imaged in cells without simultaneous excitation of NAD(P)H, an endogenous coenzyme associated with oxidative photodamage in biological specimens. Although CPNs are excited at a spectral range similar to NAD(P)H, CPNs have cross-sections approximately five orders of magnitude larger than those of native fluorescent coenzymes. These high cross-section values support the utility of CPNs as 2P probes, especially considering the invariability of CPN cross-sections over extended storage periods of at least 3 months at room temperature (RT).

Additional spectroscopic characterization of the CPNs was carried out using fluorescence lifetime microscopy (FLIM). A double-exponential decay fit of the fluorescence-lifetime data[23] resulted in the determination of two lifetimes, 0.84 ns (74%) and 1.38 ns (26%) (Fig. 1d). These values coincide well with previously published lifetimes of CPs in poor solvents.[24] The double-exponential decay may indicate the presence of two fluorescent populations with distinct aggregation states of interpolymer chains. It is also possible that there are two relaxation mechanisms even in a single CPN, depending on the fraction of CP chains being exposed to the hydrophilic environment versus the fraction residing in the hydrophobic interior. Since the average lifetimes of CPNs are 10–50 times faster than QDs, corresponding to a higher photon emission rate, CPNs are brighter than QDs.

To examine the photostability of CPN in biological systems, we incubated live BALB/C 3T3 fibroblasts with CPN and QD525

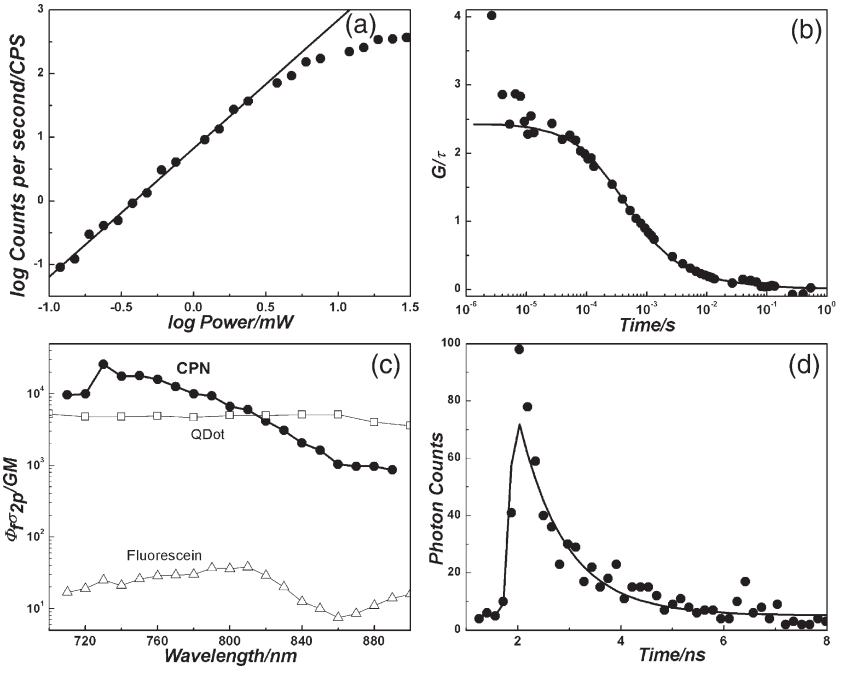

Figure 1. a) Fluorescence power dependence of CPN. The log plot of cps versus power exhibits typical 2P excitation saturation behavior at higher power. The cps rate increases as the square of the power. The fit line has a slope of 2.0. b) FCS curve for CPN (excitation power 0.5 mW at 780 nm). Fits indicate CPN radius of 3.8 nm and diffusion time of 382 μs. c) Log plot of 2P-action cross-sections versus 2P excitation wavelengths. d) Fluorescence lifetime of CPN. Raw data were fitted (solid line) using the global analysis algorithm. Lifetimes extracted were 0.84 and 1.38 ns.

(Qtracker 525, Invitrogen), respectively. Cells were fixed with paraformaldehyde, and samples were continuously imaged at 780 nm with a power of 2 mW for a 1 h period (see Supporting Information, Fig. S2a). The total dosage at each pixel was 0.1 mJ. After background rejection, the photobleaching decay curves (Fig. S2b, Supporting Information) showed that the CPNs and QD525 bleaching rates were virtually identical; CPN and QD525 retain 86% and 83% of their initial intensities, respectively. Focusing on only the 25 most intense pixels in the images, the photobleaching in these high-intensity regions is more severe in both cases with CPN and QD525 retaining 70% and 60% of the initial intensity, respectively. It is interesting to note that the brighter pixels bleach faster, which is consistent with the presence of a higher local density of reactive oxygen species. Similar photostability was observed in CPN and QD during the hour of continuous irradiation, indicating high resistance to bleaching in CPN that is comparable to QDs.

We demonstrated the use of CPNs for long-term cell tracking by monitoring capillary formation in a collagen gel-based microfluidic device.[25] Microfluidic devices are useful for examining cellular behavior in the microcellular niche due to the control of both mechanical and biochemical properties. Human adult dermal microvascular endothelial cells (HMVEC-d) were preincubated with CPNs followed by CellTracker Red before seeding into the device. Phosphate-buffered saline (PBS)-washed cells were seeded and cultured in the device over a period of four days. Within 24 h after cell seeding, a concentration gradient of vascular endothelial growth factor (VEGF) and sphingosine was set up across the collagen-gel region in order to promote capillary formation. The 2P-excitation images in Figure 2 show projection of capillary structures through 80 μm of the central gel region (the z-stack consists of 40 images at 2 μm step). Cells invade the collagen-gel region over three days and form initial sprouts that evolve into capillaries with lumens.[25] On day 1 (12 h after addition of growth factor), capillaries have started to sprout into the gel region from the cell monolayer. On day 2, it can be seen that these same capillaries have formed multiple sprouts on either side of the polydimethylsiloxane (PDMS) post (gray squares), and by day 3, these capillaries have invaded 250 μm into the gel region. The CellTracker Red outlines the extents of the sprouts and cellular structures on the monolayer as well as inside the gel region. CellTracker is a membrane-permeable fluorescent dye that diffuses into the cytosol (random distribution), while the CPNs reside mainly in vesicular structures in the cells. We expect that the probes will have certain overlaps in the cytosol (likely in endosomes or lysosomes). In addition to the overlaps, the images in Figure 2 are projections of angiogenesis in 3D, which result in the overlap of cellular structures. Over the three imaging days (and over the five days since initially added to the cells), both the CellTracker Red dye and CPN probes persist in the cells, allowing continuous tracking and monitoring. Addition of CPN probes has not stunted the growth of these capillaries, proving that cell behavior is unaffected by CPN addition, as has also been shown in previous cell-viability studies.[17] The observed nontoxicity of CPN and its longevity inside cells demonstrate its suitability as a long-term intracellular marker. These results indicate that CPNs could be useful for a broad range of applications, including understanding immune-cell trafficking in animal models[26] and monitoring implanted-stem-cell migration.[27] A loss in fluorescence intensity over time has been observed, and the exact causes of this decrease are not certain. It may be due to natural degradation, active degradation by the cells, or the dilution of CPNs due to cell division.

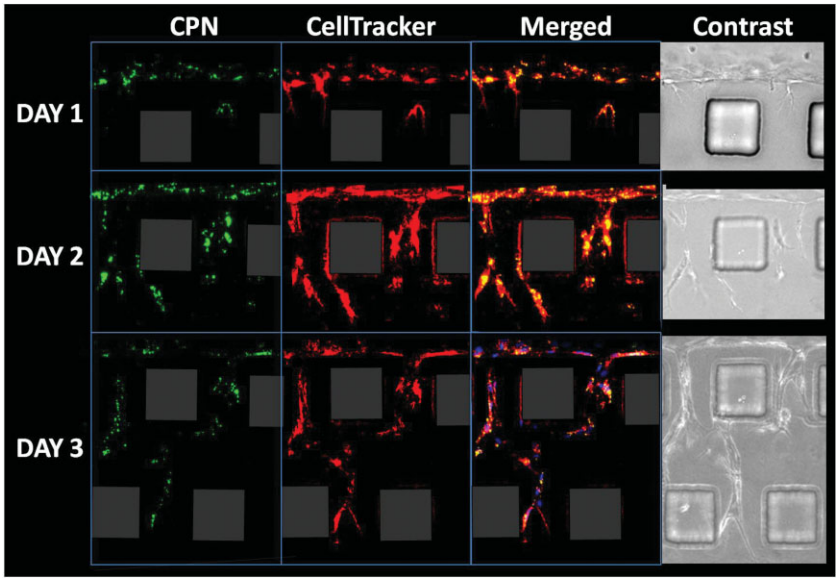

Figure 2. Fluorescence images (days 1, 2, and 3) of cultured cells in a microfluidic device. 2P-excitation images showing projection of capillary structures through 80 μm of the central gel region (the z-stack consists of 40 images at 2 μm step). Cells invade the collagen-gel region over three days and form initial sprouts that evolve into capillaries with lumens. To further demonstrate population growth of cells, the day-3 image (merged) was combined with DAPI nuclear staining (blue). The yellow color represents overlapped colors of CPNs (green) and CellTracker (red). Corresponding phase-contrast images are also shown. The gray squares in the fluorescent images were inserted for presenting posts in the device.

In this report, we have demonstrated CPNs as promising multiphoton probes useful for both biological and biomedical applications. The photophysical properties of CPNs, such as their extremely large 2P cross-section and superior photostability, compare well with those of QDs. The lack of toxic effects during long-term monitoring of capillary formation in a microfluidic device also supports the potential of CPNs for in vitro and possibly in vivo imaging applications. In addition to the superior properties of CPNs that are comparable to QDs, it is important to note the high versatility of CPN synthesis, which is the key ability to further improve probe efficiency. Higher 2P cross-sections can be obtained by employing various electronically defined (electron-rich or -deficient) monomers into the conjugated backbones. Tuning of emission wavelengths is also possible by electronic modulation that changes the π-electron conjugation length. In addition, cellular-uptake efficiency, biocompatibility, and targeting ability can be optimized by introducing various functional groups as side chains in the CPs.

Finally, novel nanoparticle fabrication methods controlling interactions between polymer chains can also improve the size and size distribution of CPNs for efficient labeling and detection in biological systems.

Experimental

2P Imaging Instrumentation: The 2P microscope is based on a modified inverted microscope, Axiovert 110 by Zeiss Inc. (Thornwood, NY), with a femtosecond laser source from the Mira family of modelocked Ti/Sapphire oscillators by Coherent Inc. (Santa Clara, CA). The laser excites a sub-femtoliter volume at the focal point of a 40× Fluor objective (1.25 NA, Zeiss, Thornwood, NY). For both FLIM and FCS, the laser is tuned at 780 nm with 0.5 mW power after the objective.

For FLIM, the signal is sent to the top port of the microscope where the signal is isolated using a HQ500LP from Chroma (Rockingham, VT). A photomultiplier tube (PMT), R7400P from Hamamatsu (Bridgewater, NJ), detects emitted photons, and this signal is sent to a time-correlated single photon counting (TCSPC) card, SPC-730 from Becker-Hickl (Berlin, Germany). For FCS, a PMT with higher photon detection efficiency, the H7421 from Hamamatsu (Bridgewater, NJ) is used in the bottom port of the microscope and is combined with single photon counting electronics.

FCS: The normalized temporal autocorrelation function, $G(\tau)$, is given by

$$G(\tau) = \frac{\langle \delta F(t) \times \delta F(t+\tau) \rangle}{\langle F(t) \rangle^2} \quad (1)$$

where $\delta F(t) = F(t) - \langle F(t) \rangle$ and $\langle F(t) \rangle = (1/T)\int_0^T F(t)\mathrm{d}t$. The autocorrelation curve is fit with the equation

$$G(\tau) = \frac{G(0)}{\left(1+\frac{t}{t_D}\right)\sqrt{1+\left(\frac{r_0}{z_0}\right)^2 \times \frac{t}{t_D}}} \quad (2)$$

which describes freely diffusing fluorescence molecules. $G(0) = 1/\langle N \rangle = 1/V_{eff}\langle C \rangle$, N is the number of particles, V_{eff} is the effective focal volume, $(r_0/z_0)^2$ is a measure of the aspect ratio of the focal volume (r_0 = radius, z_0 = height), and τ_D is the diffusion timescale of the molecules, related to the molecule diffusion constant, D, by $\tau_D = r_0^2/4D$. The FCS focal volume is calibrated using a 10 nM AlexaFluor 488 sample (Molecular Probes, OR). FCS autocorrelation curves were analyzed using MATLAB (The MathWorks, Natick, MA) using the *lsqnonlin* nonlinear least-squares curve fitting function. In addition to measuring the number of molecules in the excitation volume, FCS further provides CPN diffusivity of 66.5 $\mu m^2 s^{-1}$. From the Stokes–Einstein equation, the CPN particles' radii were calculated to be 3.8 nm (7.6 nm in diameter), nearly identical to that obtained from initial DLS measurements.

2P Action Cross-Section: The time-averaged fluorescence photon flux, $\langle F(t) \rangle$ is given by

$$\langle F(t) \rangle = \frac{1}{2}\eta C \Phi_f \sigma_{2P} g \frac{8n\langle P(t) \rangle^2}{\pi\lambda} \quad (3)$$

where η = fluorescence collection efficiency, C = sample concentration, Φ_f = fluorescence quantum efficiency, σ_{2P} = non-linear 2P absorption cross-section, g = degree of second order temporal coherence, n = index of refraction of medium lens works in, $P(t)$ = instantaneous incident power, and λ = wavelength in vacuum. The 2P action cross-section is the product $\Phi_f\,\sigma_{2P}$. Fluorescein (300 μM, pH 9) and CPN (415 nM) brightness were measured with excitation power of 10 mW and 5 mW, respectively, at 780 nm. Since fluorescein's action cross-section is known, taking the ratio of Equation 3 for both samples results in the calculation of CPN's 2P action cross-section.

FLIM: The global analysis algorithm fits all lifetime decay curves with a double-exponential decay of the form

$$I(t) = \int_0^t G(t-T)\left\{\alpha_1 e^{-T/\tau_1} + \alpha_2 e^{-T/\tau_2}\right\}\mathrm{d}T \quad (4)$$

where $I(t)$ is a convolution of the sum of the exponentials with the instrument response $G(t)$. The pre-exponential factors α_1 and α_2 reflect fractional contributions to the total fluorescence from the two populations that decay at rates τ_1 and τ_2. The code is written using MATLAB (The MathWorks, Natick, MA), and uses the *fmincon* optimization function. Convergence is defined as being reached when χ^2 varies by less than 10^{-15}.

Photobleaching: BALB/C 3T3 (ATCC, VA) cells cultured in DMEM supplemented with 10% fetal bovine serum (FBS) were incubated overnight with CPN (2.7 nM) or QD525 (10 nM), washed three times with PBS, and fixed in 4% paraformaldehyde. Samples were continuously scanned at a wavelength of 780 nm and power of 2 mW at the objective. The image frame rate was 2.5 s, and the total dosage at each pixel was 0.1 mJ.

Microfluidic Device Setup: PDMS (Silgard 184, Dow Chemical) was mixed at a curing agent/elastomer ratio of 1:10, degassed, and poured onto a silicon wafer master with geometric features as given in Figure S3 (Supporting Information). The PDMS was left to further degas at RT for 30 min and baked in the oven at 80 °C for at least 3 h before being peeled off and cut out into individual devices. Prior to cell culture, devices were sterilized in the autoclave and plasma-treated by plasma cleaner (Harrick, CA) in an air environment to increase hydrophilicity. Collagen-gel-prepolymer solution was microinjected into the device gel cage. Fluidic channels were sealed with a glass cover slip, and the gel was allowed to polymerize for 30 min in the incubator.

2P Imaging: HMVEC-d (Lonza, MD) were propagated in EGM-2MV media system with 5% FBS (LONZA, formerly Cambrex, MD). Cells were maintained in a humidified incubator at 5% CO_2 and 37 °C on collagen-coated flasks. Cells were incubated with CPN (33.2 nM) for 5 h followed by incubation with CellTracker Red (10 μM) for 30 min. Cells were washed five times with 1XPBS and suspended into a solution by trypsin treatment. Media were added to neutralize the trypsin before centrifuging at 1500 rpm for 5 min. The pellet was resuspended in media, and CPN/CellTracker Red stained cells were flowed in at a density of 2.5 million cells/mL and allowed to adhere to the gel surface. After a 24 h incubation period, devices were checked to ensure the formation of an even cell monolayer. In order to promote capillary formation, 20 ng mL^{-1} VEGF (R&D Systems, MN) was added to the monolayer channel, while in the opposite channel, 40 ng mL^{-1} VEGF and 250 nM sphingosine-1-phosphate (Sigma–Aldrich, MO) were added. 2P imaging was carried out at 24, 48, and 72 h after addition of growth factors, at a wavelength of 780 nm and power of 45 mW before a 20× Fluar objective (Zeiss, Germany). The signal was split into three channels, each with Chroma bandpass filters, 630/60, 535/40, and 470/40, selecting for red, green, and blue wavelengths, respectively. Cells were fixed with 4% paraformaldehyde and stained with 0.1% DAPI before the last imaging session for nuclear visualization. Phase-contrast images were acquired using a TE-2000U (Nikon, Japan) microscope with 20× objective.

Acknowledgements

J. H. M. acknowledges the Florida International University for Faculty Startup Funds. The authors thank Dr. R. Deans and Dr. D. Goad for critical readings of the manuscript. V. V. is supported by NIBIB (EB003805) and a research supplement grant. Supporting information is available online from Wiley InterScience or from the authors.

Received: February 5, 2009
Revised: March 4, 2009
Published online: May 12, 2009

[1] W. Denk, J. H. Strickler, W. W. Webb, *Science* **1990**, *248*, 73.
[2] M. J. Miller, S. H. Wei, I. Parker, M. D. Cahalan, *Science* **2002**, *296*, 1869.
[3] A. Agarwal, M. L. Coleno, V. P. Wallace, W. Y. Wu, C. H. Sun, B. J. Tromberg, S. C. George, *Tissue Eng.* **2001**, *7*, 191.
[4] W. Y. Jung, S. Tang, D. T. McCormic, T. Q. Xie, Y. C. Ahn, J. P. Su, I. V. Tomov, T. B. Krasieva, B. J. Tromberg, Z. P. Chen, *Opt. Lett.* **2008**, *33*, 1324.
[5] L. Fu, A. Jain, C. Cranfield, H. K. Xie, M. Gu, *J. Biomed. Opt.* **2007**, *12*, 040501.
[6] M. Albota, D. Beljonne, J. L. Bredas, J. E. Ehrlich, J. Y. Fu, A. A. Heikal, S. E. Hess, T. Kogej, M. D. Levin, S. R. Marder, D. McCord-Maughon, J. W. Perry, H. Rockel, M. Rumi, C. Subramaniam, W. W. Webb, X. L. Wu, C. Xu, *Science* **1998**, *281*, 1653.
[7] J. D. Bhawalkar, G. S. He, P. N. Prasad, *Rep. Prog. Phys.* **1996**, *59*, 1041.
[8] C. F. Wu, C. Szymanski, Z. Cain, J. McNeill, *J. Am. Chem. Soc.* **2007**, *129*, 12904.
[9] C. Wu, B. Bull, C. Szymanski, K. Christensen, J. McNeill, *ACS Nano* **2008**, *2*, 2415.
[10] L. Cao, X. Wang, M. J. Meziani, F. Lu, H. Wang, P. G. Luo, Y. Lin, B. A. Harruff, L. M. Veca, D. Murray, S. Y. Xie, Y. P. Sun, *J. Am. Chem. Soc.* **2007**, *129*, 11318.
[11] X. Michalet, F. F. Pinaud, L. A. Bentolila, J. M. Tsay, S. Doose, J. J. Li, G. Sundaresan, A. M. Wu, S. S. Gambhir, S. Weiss, *Science* **2005**, *307*, 538.
[12] J. Yao, D. R. Larson, H. D. Vishwasrao, W. R. Zipfel, W. W. Webb, *Proc. Nat. Acad. Sci. USA* **2005**, *102*, 14284.
[13] A. M. Derfus, W. C. W. Chan, S. N. Bhatia, *Nano Lett.* **2004**, *4*, 11.
[14] U. H. F. Bunz, *Chem. Rev.* **2000**, *100*, 1605.
[15] D. T. McQuade, A. E. Pullen, T. M. Swager, *Chem. Rev.* **2000**, *100*, 2537.
[16] S. W. Thomas, G. D. Joly, T. M. Swager, *Chem. Rev.* **2007**, *107*, 1339.
[17] J. H. Moon, W. McDaniel, P. MacLean, L. E. Hancock, *Angew. Chem. Int. Ed.* **2007**, *46*, 8223.
[18] R. Q. Yang, A. Garcia, D. Korystov, A. Mikhailovsky, G. C. Bazan, T. Q. Nguyen, *J. Am. Chem. Soc.* **2006**, *128*, 16532.
[19] We believe that CPNs may trap trace amount of residual acids inside the particles. The trapped acids may diffuse out during the extended storage. In the small CPN fabricated with tartaric acid, the leaching-out process significantly increases the aggregation of CPNs due to the sharply increased hydrophobic interaction between the chains. We are currently monitoring the size changes of CPNs at various concentrations and temperatures.
[20] K. M. Berland, P. T. C. So, E. Gratton, *Biophys. J.* **1995**, *68*, 694.
[21] C. Xu, W. W. Webb, *J. Opt. Soc. Am. B. Opt. Phys.* **1996**, *13*, 481.
[22] D. R. Larson, W. R. Zipfel, R. M. Williams, S. W. Clark, M. P. Bruchez, F. W. Wise, W. W. Webb, *Science* **2003**, *300*, 1434.
[23] S. Pelet, M. J. R. Previte, L. H. Laiho, P. T. C. So, *Biophys. J.* **2004**, *87*, 2807.
[24] J. H. Wosnick, C. M. Mello, T. M. Swager, *J. Am. Chem. Soc.* **2005**, *127*, 3400.
[25] V. Vickerman, J. Blundo, S. Chung, R. Kamm, *Lab Chip*, **2008**, *8*, 1468.
[26] S. Mandl, C. Schimmelpfennig, M. Edinger, R. S. Negrin, C. H. Contag, *J. Cell. Biochem.* **2002**, *S39*, 239.
[27] M. Hoehn, E. Kustermann, J. Blunk, D. Wiedermann, T. Trapp, S. Wecker, M. Focking, H. Arnold, J. Hescheler, B. K. Fleischmann, W. Schwindt, C. Buhrle, *Proc. Nat. Acad. Sci. USA* **2002**, *99*, 16267.